

Performance studies of jet flavor tagging and measurement of R_b using ParticleNet at CEPC

Libo Liao^{1,a}, Shudong Wang^{2,4}, Weimin Song³, Zhaoling Zhang³, and Gang Li^{2,b}

¹ College of Electronics and Information Engineering, Wuzhou University, 82 Fumin Third Road, Wanxiu District, Wuzhou, China

² Institute of High Energy Physics, Chinese Academy of Sciences, 19B Yuquan Road, Shijingshan District, Beijing, China

³ College of Physics, Jilin University, 2699 Qianjin Street, Changchun, China

⁴ University of Chinese Academy of Sciences, 19A Yuquan Road, Shijingshan District, Beijing, China

Received: date / Revised version: date

Abstract. Jet flavor tagging is crucial for $R_b(R_c)$ measurement, which is sensitive to testing the Standard Model and searching for new physics models. In this study, a Deep Learning method, ParticleNet, is used to enhance the efficiency of jet flavor tagging. The product of efficiency and purity of c -tagging is improved by more than 50% compared to the CEPC baseline software whose efficiency is 60%. Two methods are employed to measure $R_b(R_c)$, referred as double tagging and inverse matrix, based on the new flavor tagging approach. Both of them can improve the precision of $R_b(R_c)$, particularly for R_c , which has a 60% reduction in statistical uncertainty. In addition, the systematic uncertainties of the Monte Carlo simulation and the Deep Learning model are investigated.

1 Introduction

The measurement of the relative partial decay widths of Z boson, $R_q = \Gamma_{q\bar{q}}/\Gamma_h$, plays a crucial role in testing the Standard Model(SM) [1,2] and searching for new physics. Particularly, R_b is sensitive to the correction of Zbb vertex with new physics [3]. The decay width to a quark-antiquark final state can be expressed as [4]

$$\Gamma(Z \rightarrow q\bar{q}) = \frac{G_F M_Z^3}{2\sqrt{2}\pi} (g_{Aq}^2 R_{Aq} + g_{Vq}^2 R_{Vq}) , \quad (1)$$

where g_{Aq} and g_{Vq} are the axial and vector coupling constants, respectively, and R_{Aq} and R_{Vq} are radiation factors to account for final state Quantum Electrodynamics (QED) and Quantum Chromodynamics (QCD) corrections. The electroweak radiative corrections to the propagator and the $Zq\bar{q}$ vertex are effectively accounted for in the g_A and g_V couplings. The QED and QCD corrections at first order are flavour blind and can be represented as

$$R_{Aq} \approx R_{Vq} \approx 1 + \frac{\alpha_s(M_Z)}{\pi} , \quad (2)$$

so that the counterparts of the denominator and numerator cancel each other out in the ratio $\Gamma_{q\bar{q}}/\Gamma_h$.

The latest world averages of R_b and R_c , which are dominated by the measurements of experiments on the

LEP and the SLD [5,6,7,8,9,10], and the SM prediction of Gfitter Group [11] for R_b and R_c are shown in Table 1. It is apparent that the theoretical uncertainties are

Table 1. R_b and R_c values in experiment and theory.

	Experiment	Theory
R_b	0.21629 ± 0.00066	0.21581 ± 0.00002
R_c	0.1721 ± 0.0030	0.17221 ± 0.00003

smaller than the experimental ones by about two orders of magnitudes. So the experimental precision of $R_b(R_c)$ needs to be improved to compare with the predictions, to clarify the potential discrepancy, and to probe the physics beyond the SM.

Various approaches have been used to measure the $R_b(R_c)$, such as single tagging, double tagging, multi-tagging, etc. However, the precision was limited by the statistics and detector performance. Recently, a few electron-positron colliders, the CEPC [12], FCC-ee [13], etc, were proposed to perform precision Higgs and electroweak studies. These facilities are going to deliver huge statistics of data at Z pole, W pair threshold, and about 240 GeV to maximize the production cross section of Higgs-strahlung process, and so on. It is natural that these experiments will adopt both new detector and software technologies to achieve the best performance in the detection and reconstruction of physics objects, especially for jets.

^a liaolibo-jay@outlook.com

^b li.gang@ihep.ac.cn (corresponding author)

To measure $R_b(R_c)$, jets are essential physics objects. Therefore, good jet-clustering and tagging algorithms are key ingredients, in particular, the jet flavor tagging. Jets from different quarks or gluon have various useful characteristics. For instance, gluon jets usually have a wider energy distribution than those of quark jets, and the vertex displacements of tracks of a b jet are larger than those of other types of jet because of the longer lifetimes of bottom mesons, and several other characteristics derived from quarks or gluon are also different. These features are the basis of algorithms to tag jets.

A large number of jet tagging algorithms have been developed recently based on various approaches. For example, the LCFIPlus [14] based on BDT, is used for the International Linear Collider(ILC) [15, 16], the CEPC, and the FCC-ee physics performance study and detector optimization. The CEPC delivers great b/c -tagging performance thanks to its high precision vertex detector. The b -jets can be tagged with an efficiency of 80% at a purity of 90%. Compared with b -tagging, c -jet tagging is particularly challenging as charm hadrons have relatively shorter lifetimes than bottom ones and suffer more backgrounds. Therefore, an efficiency of 60% and a purity of 60% can be achieved for the c -jet tagging.

In this article, the performance of flavor tagging of the CEPC baseline detector is improved using a new deep learning (DL) model, ParticleNet [17]. The same method is also used for the event classification and measuring $R_b(R_c)$. In addition, another novel DL model, Particle Flow Network(PFN)[18], is used for comparison and cross check. The rest parts are organized as the following. The simulation, reconstruction software, and Monte Carlo (MC) samples are introduced in Section 2; the DL model and the results of flavor tagging are presented in Section 3; then the measurement of $R_b(R_c)$ with new methods is discussed in Section 4; and a summary is given in Section 5.

2 Detector, software, and samples

The study is based on the CEPC baseline detector, which, as shown in Fig. 1, is advanced from the International Large Detector (ILD) [19] on the ILC and optimized to meet the physics requirement of the CEPC. The baseline detector is designed according to the Particle Flow Algorithm [20], which could reap a better precision and efficiency of reconstructed objects by using the most suitable sub-detectors. From the inside out, the detector includes a silicon pixel vertex detector, a silicon tracker, a time projection chamber (TPC), a calorimetry system which includes an electromagnetic calorimeter (ECAL) and a hadronic calorimeter (HCAL) of very high granularity, and a muon detector embedded inside the return yoke of a solenoid magnet system which provides a magnetic field of 3 Tesla.

The vertex detector consists of six layers of silicon pixel sensors with excessive spatial resolution. The silicon tracker is made of 4 components, which are the Silicon Inner Tracker (SIT), the Silicon External Tracker (SET), the Forward Tracking Detector (FTD), and the End-cap

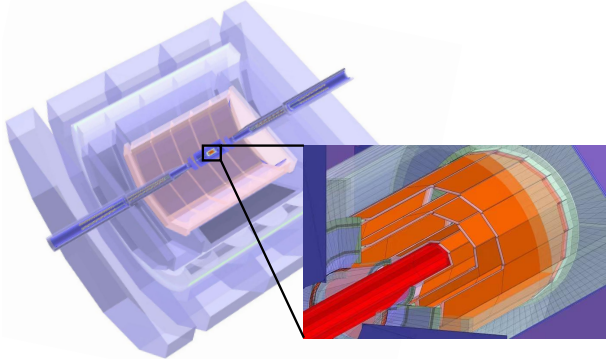


Fig. 1. The CEPC baseline detector. The left is the $r - \phi$ view of the detector. In the barrel from inside to outsize, the detector is composed of a silicon pixel vertex detector, a silicon inner tracker, a TPC, a silicon external tracker, an ECAL, an HCAL, a solenoid of 3 Tesla, and a muon detector. The right is the silicon pixel vertex detector, which consists with 3 concentric cylindrical double-layers of high spatial resolution.

Tracking Detector (ETD). The TPC is designed within the framework of the LCTPC collaboration [21]. The ECAL and HCAL are each composed of 1 barrel and 2 end-cap sections. The detailed description of the CEPC baseline detector may be seen in Ref. [12].

The MC samples for this study are produced with the CEPC full simulation, reconstruction, and analysis framework [22]. The physics processes are generated with WHIZARD 1.9.5 [23]. PYTHIA 6 [24] is then used for hadronization. MokkaPlus [25], a GEANT4-based [26] detector simulation tool, is used to model the detector response. Arbor [20] is used to reconstruct physics objects including tracks, photons, and neutral hadrons, and LCFI-Plus [14] is used to reconstruct (secondary) vertices and jets.

In this study, there are 3 hadronic decay modes of Z boson used for jet flavor tagging study, which are $e^+e^- \rightarrow Z \rightarrow b\bar{b}$, $c\bar{c}$, and $o\bar{o}(u\bar{u}/d\bar{d}/s\bar{s})$. In the measurement of $R_b(R_c)$, the main background process, $Z \rightarrow \tau\tau$, is also taken into account. For each process, 450,000 events are produced, which has 900,000 jets in total. The jets are reconstructed using $e^+e^- - k_t$ algorithm in LCFIPlus [14], where all particles, including the reconstructed primary and second vertices, are clustered into two jets.

3 Jet flavor tagging with ParticleNet

In this study, ParticleNet is used as the nominal model and PFN as a comparison and cross check.

Based on the particle cloud representation, which treats a jet as an unordered group of particles, an effective model, ParticleNet, has been developed. It is a customized neural network model using Dynamic Graph Convolutional Neural Network (DGCNN) [27] for jet tagging.

ParticleNet has several advantages. First, it can deal with the varying number of particles in a event, which is common in experimental high energy physics. Second,

the model is designed to respect the particle permutation invariance, which makes a natural and promising representation of jets. Third, ParticleNet makes extensive use of EdgeConv [27] operations to update the graph representation dynamically for better performance. Last but not least, ParticleNet could exploit local neighborhood information explicitly while most of the other DL models could only use global symmetric features.

3.1 Deep learning models and configuration

ParticleNet model used in this paper consists of three EdgeConv blocks, a global average pooling layer and two fully connected layers. The number of channels C for each EdgeConv block is (64, 64, 64), (128, 128, 128), and (256, 256, 256), respectively. After the EdgeConv blocks, a channel-wise [28] global average pooling operation is applied to aggregate the learned features over all particles in the cloud. This is followed by a fully connected layer with 256 units and the ReLU activation [29]. A dropout layer [30] with a drop probability of 0.1 is included to prevent overfitting. A fully connected layer with N units, followed by a softmax function, is used to generate the output, where the N is the number of categories in the classification task. For the number of nearest neighbors k for all three blocks, some optimization is performed, which indicates that 12 for jet tagging and 16 for event classification are optimal. The configuration of PFN is directly taken from the Ref. [18], since it is only used for cross check.

3.2 Visualizing the data sets

Jet flavor tagging algorithm is based on features of the data sets. In this study, these features could be categorized into three types. The first is the jet kinematics, such as the intermediate hadrons, multiplicity, and momentum distribution, etc. The second is impact parameters of the charged tracks, which are very informative for b -tagging. The last one is types of particles in a jet, i.e. particle identification (PID). Considering three types of jets to be studied, some distributions are shown in Fig. 2. Figure 2(a) is the multiplicity versus momenta of tracks, where it can be seen that the number of tracks of b jets is slightly larger than those of c jets and light (o) jets, which is consistent with the decay properties of heavier B hadrons. The distribution of impact parameters versus momenta is shown in Fig. 2(b). Clear patterns can be observed: b jets have significant contribution of larger impact parameters and of energetic tracks compared with c and o jets. Figure 2(c) shows the weighted fractions of different particle types in the three physics processes. It is clear that b quarks produce more energetic leptons, c quarks produce slightly more energetic kaons.

In the event classification, the main background process is $e^+e^- \rightarrow Z \rightarrow \tau^+\tau^-$. This background has rather different features, obviously, compared with the signal, i.e. $e^+e^- \rightarrow b\bar{b}, c\bar{c}$ and $o\bar{o}$, as shown in Fig. 3. It indicates that the background has significantly less multiplicity and higher momenta of tracks.

3.3 Training and evaluation

Both ParticleNet and PFN are implemented and running with 8 Intel® Xeon® Gold 6240 CPU cores and 4 NVIDIA® Tesla® V100-SXM2-32GB GPU cards at the IHEP GPU farm. During model training, the common properties of the neural networks include a categorical cross-entropy loss function, the Adam optimization algorithm [31], a batch size of 1,024, a starting learning rate of 0.005. 900,000 jets are used for each production mode, and the total number of jets of 3 decays is 2,700,000. The full data-set is split into training, validation, and test samples according to the fraction of 7:1.5:1.5. The monitoring of loss and accuracy on training and validation shows that the models converge well and there is no obvious over-training after 30 epochs.

The computation consumption of ParticleNet and PFN models could be estimated. Only total consumption of GPU and CPU is used for estimation, since all the computing resources could only be accessed indirectly via a workload manager server. ParticleNet takes about 190 minutes for training (30 epochs) and 3 minutes for inference. PFN takes about 30 minutes for training (80 epochs) and less a minute for inference. Both two methods could be finished on a reasonable time scale.

3.4 Performance

Both ParticleNet and PFN outperform than the LCFIPlus in terms of jet flavor tagging. The accuracy of two novel models are summarized in Table 2, together with those in Ref. [32]. ParticleNet could achieve accuracy of about 87.6%, which is at least 9% better than those in Ref. [32].

Figure 4(a) shows the confusion matrix with ParticleNet and Fig. 4(b) is the Receiver Operating Characteristic (ROC) curves, another metric to demonstrate the performance of a classifier. The numerical results of efficiencies and Area Under Curve (AUC) of both models in different jet tagging are listed in Table 3. The efficiencies, also called recalls, are determined by taking the largest score of a jet predicted by the classifiers, which are same as the corresponding diagonal terms of the confusion matrix. It can be seen that the performance of b -tagging is always better than c - and o -tagging. This observation is consistent with the results in Ref. [32].

The performance of ParticleNet and PFN are generally better than those in Ref. [32]. This could be explained from two sides, one is that much richer information of a jet is used including four momenta, impact parameters, and PIDs, the other is that ParticleNet and PFN have strong inductive bias for representing high energy events. ParticleNet outperforms PFN, which is consistent with the study in Ref. [17], and the authors explained that "the Deep Sets(PFN) approach does not explicitly exploit the local spatial structure of particle clouds, but only processes the particle clouds in a global way."

To demonstrate the physics impacts of flavor tagging, a detailed comparison in terms of the product of efficiency and purity, $\epsilon\rho$, is performed. Taking the measurement of

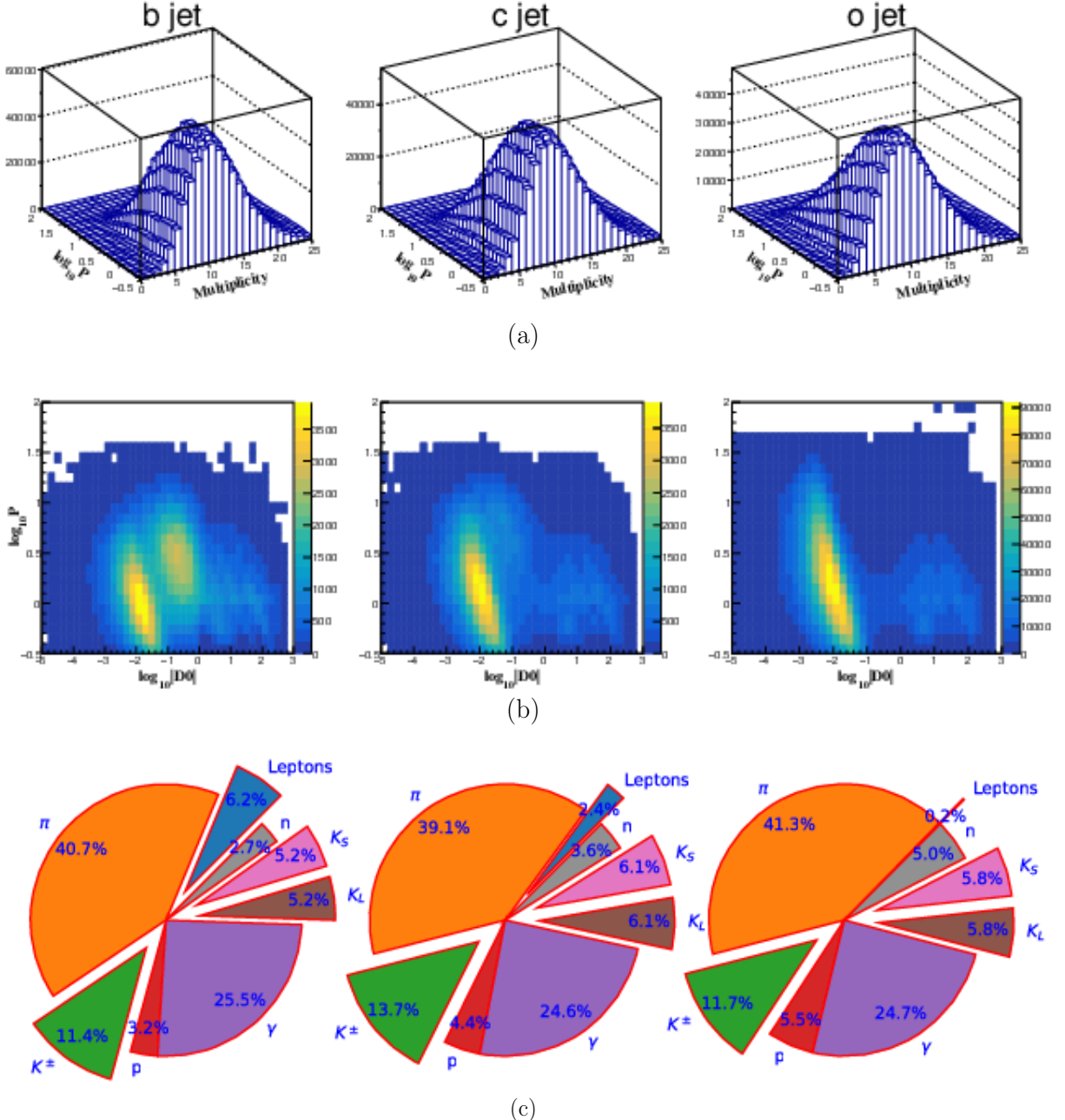


Fig. 2. The feature plots of b, c , and o in jet level. The 2-dimensional diagram of charged multiplicity versus momentum distribution is shown in the top panel; the 2-dimensional diagrams of momentum versus $D0$ are shown in the middle panel; the fractions of all particle types in $b\bar{b}$, $c\bar{c}$, and $o\bar{o}$ weighted by momentum in the bottom panel, where the PID is based on the MC truth.

$R_b(R_c)$ as an example, the Eq. 3 gives the connection between its statistical uncertainty and $\epsilon\rho$. It is known for decades that to maximize $\epsilon\rho$ is identical to minimize the statistical uncertainties.

$$(\Delta R_i)^2 \propto \frac{1}{\epsilon_i \rho_i}. \quad (3)$$

To compare the performance of various flavor tagging methods, some working points are chosen. The Table 4 summarizes the numerical results, where LCFIPlus and

XGBoost are taken as references. The table shows that in terms of the product of efficiency and purity, the performance of ParticleNet is much better than the others, especially in c -tagging. ParticleNet is more than 50% better compared with LCFIPlus when the efficiency of c -tagging is 60%. A specific example to illustrate the impact is that ParticleNet could improve the statistical uncertainty in counting c jets by 30% compared with the XGBoost. PFN

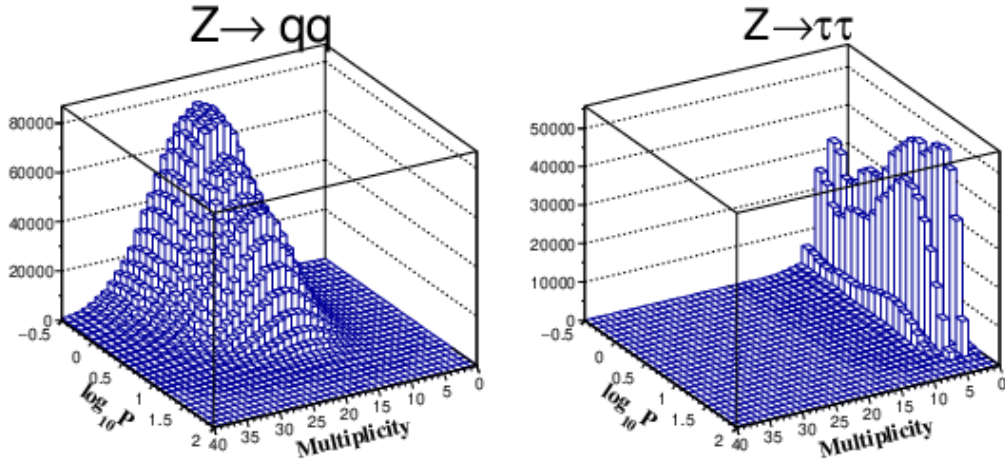


Fig. 3. The 2-dimensional histogram of charged multiplicity versus momentum distribution. The left one is $Z \rightarrow q\bar{q}$ channel. The right is $Z \rightarrow \tau\bar{\tau}$ channel.

Table 2. The accuracy of different methods for flavor tagging. In this study, ParticleNet is trained 9 times using randomly initialized weights and the result from the median-accuracy are shown, while PFN is trained only once and the uncertainty from randomly initialized weights is negligible.

Algorithm	ParticleNet	PFN	DNN	BDT	GBDT	gforest	XGBoost
Accuracy	0.876	0.850	0.788	0.776	0.794	0.785	0.801

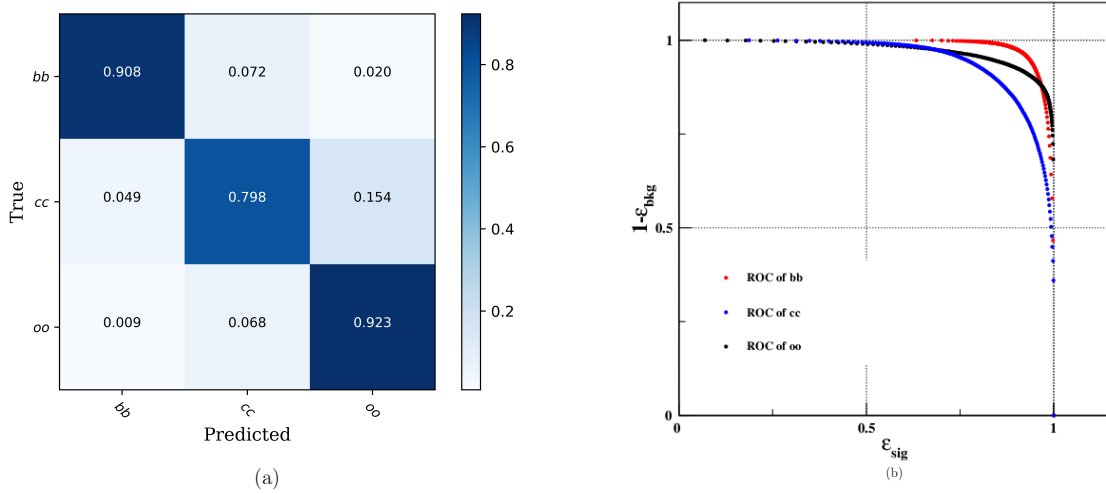


Fig. 4. The (a) confusion matrix and (b) ROCs of jet tagging with ParticleNet. oo means the light quark pairs, $u\bar{u}$, $d\bar{d}$, and $s\bar{s}$. The training is repeated 9 times using randomly initialized weights. The plots show the results from the median-accuracy training.

also achieves comparable improvement and confirms the correctness of ParticleNet.

4 Measurement of relative decay width

In the LEP, R_b is measured with various methods, which are based on counting the events with either one or both hemisphere tagged. In this study, jet is akin to hemisphere

in LEP and it would be used in the rest of this paper. The observed number of jets of flavor i (single tag), $N_s^{i,\text{obs}}$, and the observed number of jet pairs (double tag), $N_d^{i,\text{obs}}$, are given by:

$$\begin{aligned}
 N_s^{i,\text{obs}} &= 2N^{h,\text{pro}} \cdot (R_b \epsilon_{ib} + R_c \epsilon_{ic} + R_o \epsilon_{io}) , \\
 N_d^{i,\text{obs}} &= N^{h,\text{pro}} \cdot [R_b \epsilon_{ib}^2 (1 + C_{ib}) + R_c \epsilon_{ic}^2 (1 + C_{ic}) \\
 &\quad + R_o \epsilon_{io}^2 (1 + C_{io})] ,
 \end{aligned} \tag{4}$$

Table 3. The performance of ParticleNet and PFN in jet tagging. ParticleNet is trained 9 times using randomly initialized weights and the one with median-accuracy is taken.

tag	ParticleNet		PFN	
	Efficiency	AUC	Efficiency	AUC
b	0.908	0.986	0.870	0.979
c	0.798	0.951	0.765	0.930
o	0.923	0.974	0.911	0.966

Table 4. The performance of specific method in different working points, where the results of LCFIPlus are reported in Ref. [12], and the results of XGBoost are reported in Ref. [32]

tag	$\epsilon_S(\%)$	$\epsilon \times \rho$			
		LCFIPlus	XGBoost	ParticleNet	PFN
b	80	-	0.747	0.786	0.763
	90	0.72	0.713	0.821	0.752
c	60	0.36	-	0.554	0.485
	70	-	-	0.605	0.497
	80	-	0.345	0.597	0.467
	90	-	0.292	0.532	0.402

where $i(j) = b, c, o$ are flavors of jets, C_{ij} is the correlation between a jet pair of flavor j when both are tagged as i , ϵ_{ij} is the efficiency of a j jet being tagged as a i jet, $N^{h,\text{pro}}$ is total number of Z hadronic events produced in collisions, R_i is the relative decay widths of Z to jet pair of i .

R_c measurement is more challenging than R_b , since the c -tagging has less efficiency and less purity than b -tagging. Therefore, several methods are employed, such as double tag measurement, charm counting, etc. In fact, the key ingredient of a relative partial width measurement is classifying the signal and background correctly. Here a novel analysis method is proposed in terms of event classification, as a natural result of advancements in DL. This method would treat each event as a whole, which means that much richer information could be used simultaneously and that jet clustering is not necessary.

The same data sets are used for event classification, and the main SM background process $Z \rightarrow \tau\tau$ is taken into account in this case. For each process, 450,000 events are used, and the total number of events is 1,800,000.

The results of event classification with ParticleNet are shown in Fig. 5 and Table 5 (results of PFN are also listed for comparison). It can be seen that the efficiency of event classification is higher than that of jet tagging, which is intelligible that more information is applied in events than those in jets.

To measure $R_b(R_c)$, two methods can be applied. The first is solving the Equations (4) to get $R_b(R_c)$ ($R_o = 1 - R_b - R_c$ by definition) when a working point is determined. All the ϵ_{ij} could be determined by MC simulation and the correlation between jets could be neglected temporarily. Signal regions of b , c , and o candidates are defined as the red lines, i.e, working point, in Fig. 6. There are 2 equations for each region, and 6 in total. As over-determined equations, they could be solved by the least square method. Using the same integrated luminosity as-

Table 5. The performance of ParticleNet and PFN in event classification. ParticleNet is trained 9 times using randomly initialized weights and the results from the median-accuracy is taken.

tag	ParticleNet		PFN	
	Efficiency	AUC	Efficiency	AUC
b	0.964	0.998	0.930	0.993
c	0.909	0.990	0.832	0.976
o	0.955	0.995	0.945	0.992

sumed in Ref. [33], a toy MC approach is used to calculate statistical uncertainty of $R_b(R_c)$. A total number of 10^{11} Z hadronic decay events is sampled according to Poisson distribution, and then this number is sampled into three categories, $b\bar{b}$, $c\bar{c}$, and $o\bar{o}$, according to multinomial distribution. The detection and selection procedures are also simulated according to multinomial distribution. Finally, three observed numbers are obtained by adding sampling results. Now $R_b(R_c)$ could be calculated with the least square method, as well as its statistical uncertainty.

An alternative method, named inverse matrix, is solving the equations of the confusion matrix (ϵ_{ij}) and observed numbers of signal candidates (n_i) to determined $R_b(R_c)$, as shown in Equation (5).

$$\begin{pmatrix} n_1 \\ n_2 \\ n_3 \end{pmatrix} = \begin{pmatrix} \epsilon_{11} & \epsilon_{12} & \epsilon_{13} \\ \epsilon_{21} & \epsilon_{22} & \epsilon_{23} \\ \epsilon_{31} & \epsilon_{32} & \epsilon_{33} \end{pmatrix} \begin{pmatrix} N_1 \\ N_2 \\ N_3 \end{pmatrix}, \quad (5)$$

where N_i is the number of produced events of each channel. Therefore, $R_q = N_i / \sum N_i$ could be measured simultaneously. Using the same toy MC simulation, similar precision is achieved.

The results of the two methods are summarized in Table 6. The measurements of the LEP/SLD [10] and Ref. [33] also listed for comparison. The uncertainties of relative decay width in LEP/SLD [10] are mainly limited by the statistics. The template fit [33] got excellent precision, which has the advantages of much larger statistics and more information used. The double tag and inverse matrix methods also achieve comparable precision as the template fit on R_b , but the precision of R_c is improved by almost 60%, since the DL model has much better c -tagging efficiency compared with that of the LCFIPlus.

Table 6. Statistical uncertainties (10^{-6}) of relative decay widths. The results of LEP/SLD and template fit are reported in Ref. [10] and Ref. [33]

	σ_{R_b}	σ_{R_c}	σ_{R_o}
LEP+SLD	659	3015	-
Template fit	1.2	2.3	2.1
Double tag	1.3	1.4	-
Inverse matrix	1.4	1.4	-

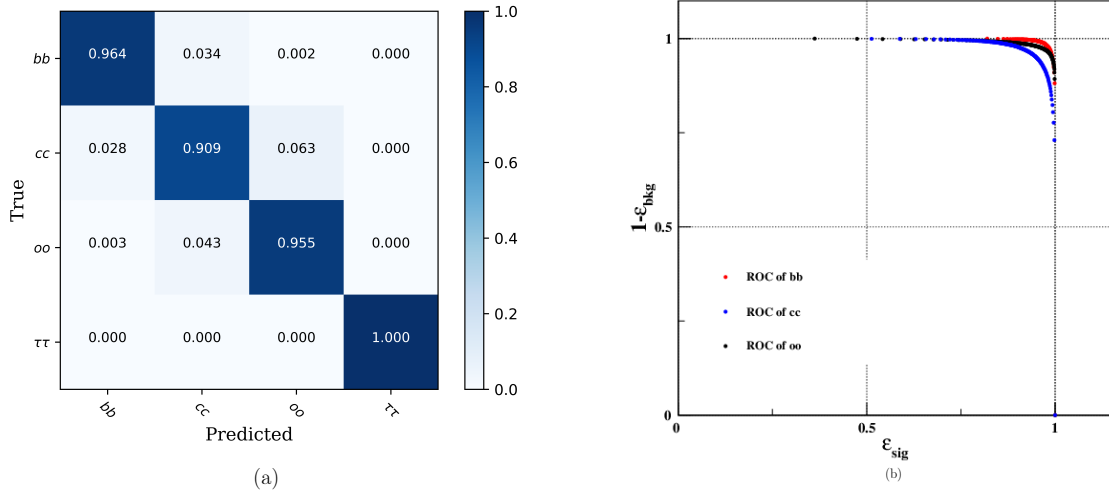


Fig. 5. The (a) confusion matrix and (b) ROCs of event-tagging with ParticleNet. The training is repeated 9 times using randomly initialized weights. The plots show the results from the median-accuracy training.

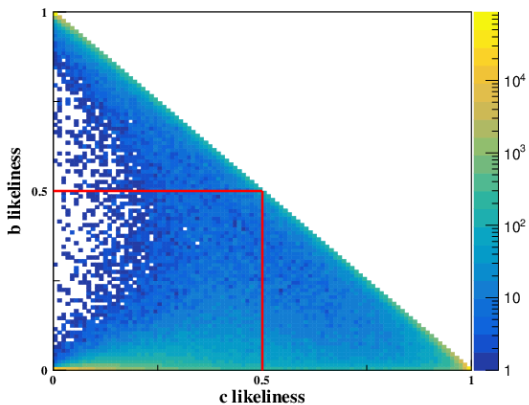


Fig. 6. The two-dimensional distribution of b -likeness versus c -likeness, where the red lines indicate one of the jet classifications. The upper left triangle is candidate area of b , the lower left rectangle is candidate area of o , and the lower right triangle is candidate area of c .

Systematic uncertainties Relative decay width is specified as a ratio, as mentioned in the introduction, and many systematic uncertainties may vanish. The systematic uncertainties are still dominant at CEPC and FCC-ee, however, since the statistical uncertainties would be improved by orders of magnitudes with huge statistics. The residual systematic uncertainties arise mainly through the quantities calculated using MC simulation, such as efficiencies, the correlations between the quarks in a event, and the DL model, etc.

Compared with the LEP era, the systematic uncertainties of efficiencies arisen by MC models, such as the lifetimes of long-lived hadrons, the branching ratios, and so on, will be improved significantly. Those quantities are intensively studied, so many new decay modes have been

discovered and uncertainties of the existing decay modes have been improved a lot. When these updates are implemented in the generators in the future, the associated systematic uncertainties could be reduced by orders of magnitude.

The correlation between jets could be reduced when tagging efficiencies have been improved. In addition, in the second method of $R_b(R_c)$ measurement, an event is taken as a global object without jet-clustering. Therefore, the systematic uncertainty due to the correlation disappears. In the studies of the LEP/SLD experiments [5, 6, 7, 8, 9], this systematic uncertainty is an important item and estimated from 2.7×10^{-4} to 6.7×10^{-3} , depending on the methods used. As a conclusion, two methods used in this study could reduce this systematic uncertainty or avoid it.

For the systematic uncertainties, they are usually arose by the input kinematic variables and the hyper-parameters. The effects of the input kinematic variables can be evaluated by changing detector coverage and resolutions, because the DL model takes the particle level information as input directly. To enlarge the statistics, fast simulation is used to generated 4 times larger samples than full simulation. The nominal samples are simulated according to the performance of the CEPC baseline detector in CDR. Alternative samples are generated by varying the momentum resolution by 10%, resolutions of impact parameters by 1%, and detector coverage by 0.1% to estimated the systematic uncertainties of detection effect. The results are summarized in Table 7. Benefited from the excellent resolutions and efficiency of the baseline detector, the impacts of changing of momenta resolution and detector coverage are under control. But for the impact parameters, the systematic uncertainty of R_c is larger than it of R_b . The reason could be that the charm mesons have relatively shorter life-times and smaller vertex displacement, which makes c -tagging strongly depend on the precision

Table 7. The summary of the systematic uncertainties of the detector resolutions and hyper-parameters of ParticleNet.

	range	$\Delta R_b(10^{-4})$	$\Delta R_c(10^{-4})$
Momenta resolution($\delta p/p$)	10%	0.30	0.34
Detector coverage($ \cos \theta $)	0.994 – 0.995	0.69	0.86
Impact parameters($\delta z/z, \delta r/r$)	1%	0.27	2.5
Number of EdgeConv blocks	2-4	2.4	3.9
Parameter of k -NN	14-18	2.8	4.5
Number of units of fully connected layer	226-286	1.2	5.4

of impact parameters. Hence, the specific commission and alignment of the vertex detector are very challenging and crucial for controlling this systematic uncertainty in future, because that the precision of CEPC vertex detector could reach micron-level. It should be noticed that the uncertainty of PID is not discussed in this research, because this is a new feature in the design stage and the detailed performance is not finalized yet.

The systematic uncertainties caused by DL model are also estimated by changing its hyper-parameters. The number of EdgeConv blocks is changed by 1, the number of neighbors required by k -NN is changed by 2, and the number of units of a fully connected layer is changed by 30, the summarized results are also shown in Table 7. The model uncertainties are at the same order for R_b and R_c , while those of R_c are slightly larger than R_b .

In conclusion, the systematic uncertainties of detector resolutions and coverage are estimated to be at 10^{-5} level, and ones of the DL model at 10^{-4} level, which are much larger than the statistical uncertainties. In future studies, the total systematic uncertainty of $R_b(R_c)$ could be improved by several ways. The MC simulation can be improved by implementing the recent measurements of long-lived particle lifetimes, branching ratios, and masses, etc. The systematic uncertainty of impact parameters could be reduced using data-driven method to tune MC simulation. The correlation between two jets certainly could be improved by theoretical calculation. But it is worth to note that this systematic uncertainty could be avoided in the inverse matrix method.

5 Summary and discussion

In this study, DL methods are used to enhance the performance of jet flavor tagging. Graph neural networks could achieve significant improvement on jet flavor tagging, especially on c -tagging. In terms of product of purity and efficiency, the c -tagging is improved more than 50% compared to the CEPC baseline software, LCFIPlus, when efficiency of c -tagging is 60%. It's understandable that ParticleNet achieves significantly better performance. Compared to the traditional methods, ParticleNet could maximize the usage of information in a jet or an event, because all the information is used as input, such as momenta, energies, and impact parameters. On the other hand, the point-cloud (set) representation, which preserves some important symmetries, has better expressive power for high energy events [34].

To demonstrate the physics impacts of these two tagging methods, $R_b(R_c)$ is taken as a test bed. Firstly, the double tagging method shows that the precision of R_c can be improved by a factor of 1.6, compared with that in Ref. [33]. Second, a new method is proposed, named inverse matrix, which can achieve comparable statistical precision as those of the first one and avoid the important systematic uncertainty caused by the correlation between two jets.

According to the study in Ref. [35], precision R_b measurement could be extremely sensitive to the modifications on the g_{Lb} and g_{Rb} couplings by new physics, because of the strong correlation between δg_{Lb} and δg_{Rb} . For more details, see the Ref. [35].

The main systematic uncertainties of $R_b(R_c)$ measurement with high statistics are investigated, in particular on detector resolutions and the DL model. As a preliminary conclusion, the systematic uncertainties are generally one or two orders of magnitudes larger than this of statistical uncertainty. Dealing with systematic uncertainty of the analysis with huge statistics will be rather challenging in future. Fortunately, huge statistics also make data-driven feasible to calibrate the MC simulation precisely. And studies on systematic uncertainty associated with DL methods are hot spot and advancing very fast. Hence, It is promising that all the systematic uncertainties could be reduced in future with more data added and development of new approaches.

Acknowledgements This work is supported by the National Natural Science Foundation of China (NSFC) (12075271, 12047569).

References

1. S. L. Glashow, Partial Symmetries of Weak Interactions. *Nucl. Phys.* **22**, 579-588 (1961). [https://doi.org/10.1016/0029-5582\(61\)90469-2](https://doi.org/10.1016/0029-5582(61)90469-2)
2. S. Weinberg, A Model of Leptons. *Phys. Rev. Lett.* **19**, 1264-1266 (1967). <https://doi.org/10.1103/PhysRevLett.19.1264>
3. J. R. Ellis, J. L. Lopez and D. V. Nanopoulos, Supersymmetry, supergravity and R(b) revisited in the light of LEP-2. *Phys. Lett. B* **397**, 88-93 (1997). [https://doi.org/10.1016/S0370-2693\(97\)00156-1](https://doi.org/10.1016/S0370-2693(97)00156-1). [arXiv:hep-ph/9612376](https://arxiv.org/abs/hep-ph/9612376) [hep-ph]
4. M. I. Vysotsky, V. A. Novikov, L. B. Okun and A. N. Rozanov, Electroweak radiative corrections

in Z boson decays. *Phys. Usp.* **39**, 503-538 (1996). <https://doi.org/10.1070/PU1996v03n05ABEH000146>. [arXiv:hep-ph/9606253](https://arxiv.org/abs/hep-ph/9606253) [hep-ph]

5. M. Acciarri *et al.* [L3], Measurement of $R(b)$ and $\text{Br}(b \rightarrow \text{lepton neutrino } X)$ at LEP using double tag methods. *Eur. Phys. J. C* **13**, 47-61 (2000). <https://doi.org/10.1007/s100520000296>. [arXiv:hep-ex/9909045](https://arxiv.org/abs/hep-ex/9909045) [hep-ex]
6. G. Abbiendi *et al.* [OPAL], A Measurement of $R(b)$ using a double tagging method. *Eur. Phys. J. C* **8**, 217-239 (1999). <https://doi.org/10.1007/s100529901087>. [arXiv:hep-ex/9810002](https://arxiv.org/abs/hep-ex/9810002) [hep-ex]
7. P. Abreu *et al.* [DELPHI], A Precise measurement of the partial decay width ratio $R(b)^{**0} = \text{Gamma}(b \text{ anti-} b) / \text{Gamma}(\text{had})$. *Eur. Phys. J. C* **10**, 415-442 (1999). <https://doi.org/10.1007/s100520050766>
8. R. Barate *et al.* [ALEPH], A Measurement of $R(b)$ using mutually exclusive tags. *Phys. Lett. B* **401**, 163-175 (1997). [https://doi.org/10.1016/S0370-2693\(97\)00407-3](https://doi.org/10.1016/S0370-2693(97)00407-3)
9. K. Abe *et al.* [SLD], Measurement of the branching ratio of the $Z0$ into heavy quarks. *Phys. Rev. D* **71**, 112004 (2005). <https://doi.org/10.1103/PhysRevD.71.112004>. [arXiv:hep-ex/0503005](https://arxiv.org/abs/hep-ex/0503005) [hep-ex]
10. S. Schael *et al.* [ALEPH, DELPHI, L3, OPAL, SLD, LEP Electroweak Working Group, SLD Electroweak Group and SLD Heavy Flavour Group], Precision electroweak measurements on the Z resonance. *Phys. Rept.* **427**, 257-454 (2006). <https://doi.org/10.1016/j.physrep.2005.12.006>. [arXiv:hep-ex/0509008](https://arxiv.org/abs/hep-ex/0509008) [hep-ex]
11. J. Haller, A. Hoecker, R. Kogler, K. Mönig, T. Peiffer and J. Stelzer, Update of the global electroweak fit and constraints on two-Higgs-doublet models. *Eur. Phys. J. C* **78**, no.8, 675 (2018). <https://doi.org/10.1140/epjc/s10052-018-6131-3>. [arXiv:1803.01853](https://arxiv.org/abs/1803.01853) [hep-ph]
12. CEPC Study Group, CEPC Conceptual Design Report: Volume 2 - Physics & Detector (2018). [arXiv:1811.10545](https://arxiv.org/abs/1811.10545)
13. A. Abada *et al.* [FCC], FCC-ee: The Lepton Collider: Future Circular Collider Conceptual Design Report Volume 2. *Eur. Phys. J. ST* **228**, no.2, 261-623 (2019). <https://doi.org/10.1140/epjst/e2019-900045-4>
14. Taikan Suehara, Tomohiko Tanabe, LCFIPlus, A Framework for jet Analysis in Linear Collider Studies. [arXiv:1506.08371](https://arxiv.org/abs/1506.08371) [physics.ins-det]
15. C. Adolphsen, M. Barone, B. Barish, K. Buesser, P. Burrows, J. Carwardine, J. Clark, H. Mainaud Durand, G. Dugan and E. Elsen, *et al.*, The International Linear Collider Technical Design Report - Volume 3.I: Accelerator & in the Technical Design Phase. [arXiv:1306.6353](https://arxiv.org/abs/1306.6353) [physics.acc-ph]
16. C. Adolphsen, M. Barone, B. Barish, K. Buesser, P. Burrows, J. Carwardine, J. Clark, H. Mainaud Durand, G. Dugan and E. Elsen, *et al.*, The International Linear Collider Technical Design Report - Volume 3.II: Accelerator Baseline Design. [arXiv:1306.6328](https://arxiv.org/abs/1306.6328) [physics.acc-ph]
17. H. Qu and L. Gouskos, ParticleNet: Jet Tagging via Particle Clouds. *Phys. Rev. D* **101**, no.5, 056019 (2020). <https://doi.org/10.1103/PhysRevD.101.056019>. [arXiv:1902.08570](https://arxiv.org/abs/1902.08570) [hep-ph]
18. P. T. Komiske, E. M. Metodiev and J. Thaler, Energy Flow Networks: Deep Sets for Particle Jets. *JHEP* **01**, 121 (2019). [https://doi.org/10.1007/JHEP01\(2019\)121](https://doi.org/10.1007/JHEP01(2019)121). [arXiv:1810.05165](https://arxiv.org/abs/1810.05165) [hep-ph]
19. T. Behnke, J. E. Brau, P. N. Burrows, J. Fuster, M. Peskin, M. Stanitzki, Y. Sugimoto, S. Yamada, H. Yamamoto and H. Abramowicz, *et al.*, The International Linear Collider Technical Design Report - Volume 4: Detectors. [arXiv:1306.6329](https://arxiv.org/abs/1306.6329) [physics.ins-det]
20. M. Ruan and H. Videau, Arbor, a new approach of the Particle Flow Algorithm. [arXiv:1403.4784](https://arxiv.org/abs/1403.4784) [physics.ins-det]
21. LCTPC collaboration. <https://www.lctpc.org/>
22. M. Ruan, H. Zhao, G. Li, C. Fu, Z. Wang, X. Lou, D. Yu, V. Boudry, H. Videau and V. Balagura, *et al.* Reconstruction of physics objects at the Circular Electron Positron Collider with Arbor. *Eur. Phys. J. C* **78**, no.5, 426 (2018). <https://doi.org/10.1140/epjc/s10052-018-5876-z>. [arXiv:1806.04879](https://arxiv.org/abs/1806.04879) [hep-ex]
23. Kilian, W., Ohl, T. & Reuter, J., WHIZARD - simulating multi-particle processes at LHC and ILC. *Eur. Phys. J. C* **71**, 1742 (2011). <https://doi.org/10.1140/epjc/s10052-011-1742-y>
24. T. Sjostrand, S. Mrenna and P. Z. Skands, PYTHIA 6.4 Physics and Manual. *JHEP* **05**, 026 (2006). <https://doi.org/10.1088/1126-6708/2006/05/026>. [arXiv:0603175](https://arxiv.org/abs/0603175)
25. P. Moras de Freitas *et al.*, MOKKA: A detailed Geant4 simulation for the international linear collider detectors. <https://flcwiki.desy.de/Mokka>
26. S. Agostinelli *et al.* [GEANT4], GEANT4-a simulation toolkit. *Nucl. Instrum. Meth. A* **506**, 250-303 (2003). [https://doi.org/10.1016/S0168-9002\(03\)01368-8](https://doi.org/10.1016/S0168-9002(03)01368-8)
27. Y. Wang, Y. Sun, Z. Liu, S. E. Sarma, M. M. Bronstein and J. M. Solomon, Dynamic graph cnn for learning on point clouds. *ACM Trans. Graph.* **38**, 146 (2019).
28. Gao, Hongyang, Zhengyang Wang and Shuiwang Ji, ChannelNets: Compact and Efficient Convolutional Neural Networks via Channel-Wise Convolutions. in *IEEE Transactions on Pattern Analysis and Machine Intelligence* **43** (2021): 2570-2581.
29. X. Glorot, A. Bordes, and Y. Bengio, Deep sparse rec- tifier neural networks. in Proceedings of the Fourteenth International Conference on Artificial Intelligence and Statistics, Vol. 15 (PMLR, Fort Lauderdale, FL, USA, 2011) pp. 315–323.
30. N. Srivastava, G. Hinton, A. Krizhevsky, I. Sutskever, and R. Salakhutdinov, Dropout: A simple way to prevent neural networks from overfitting. *Journal of Machine Learning Research* **15**, 1929–1958 (2014).
31. Diederik P. Kingma and Jimmy Ba, Adam: A Method for Stochastic Optimization. *CoRR* (2015). [arXiv:1412.6980](https://arxiv.org/abs/1412.6980)
32. Fan Yang, Flavor Tagging Using Machine Learning Algorithms. 2017.
33. B. Li, Y. Du, Z. Liang and B. Liu, Performance study of the relative decay width measurement in hadronic decays of Z boson at CEPC by using the template method. *Int. J. Mod. Phys. A* **36**, no.27, 2150207 (2021). <https://doi.org/10.1142/S0217751X21502079>
34. C. Li, H. Qu, S. Qian, Q. Meng, S. Gong, J. Zhang, T. Y. Liu and Q. Li, Does Lorentz-symmetric design boost network performance in jet physics?. [arXiv:2208.07814](https://arxiv.org/abs/2208.07814) [hep-ph]
35. S. Gori, J. Gu and L. T. Wang, The $Zb\bar{b}$ couplings at future $e^+ e^-$ colliders. *JHEP* **04**, 062 (2016). [https://doi.org/10.1007/JHEP04\(2016\)062](https://doi.org/10.1007/JHEP04(2016)062). [arXiv:1508.07010](https://arxiv.org/abs/1508.07010) [hep-ph]